GAS JET IMPINGING ON LIQUID SURFACE: CAVITY SHAPE MODELLING AND VIDEO-BASED ESTIMATION

Magnus Evestedt and Alexander Medvedev

Department of Information Technology, Uppsala University,
P. O. Box 337, SE-951 05, SWEDEN

Abstract: A water model is studied to simulate physical phenomena in the LD steel converter. The depression in the liquid, due to the impinging gas jet, is measured by means of a video camera. Image processing tools together with a nonlinear mathematical model based on the physics of the liquid-gas system, are used to describe the cavity profile. The properties of the model are investigated. A quantification of the uncertainty of the cavity depth estimates is given and the frequency content of the oscillations of the indentation profile is characterized by using the Fast Fourier Transform.

Keywords: Modelling, Estimation, Image processing

1. INTRODUCTION

A jet of gas impinging on the surface of a liquid has many industrial applications. The focus of this paper is on a steel making process involving top blowing *e. g.* the LD converter. It is widely used and stands for approximately 60% of the total world steel production.

The main idea in the LD process is to reduce, by oxidization, the contents of carbon, silicon and other contaminating components in the molten metal. In the LD converter, oxygen is jetted onto the liquid iron surface from the top, through a lance, at supersonic speed. In the interaction area between the gas and the liquid, a cavity is formed, where some of the oxidization occur. The jetting also produces slag, where much of the process' chemical reactions take place.

Understanding the effects of a gas jet impinging on a liquid surface would give more insight into the process behavior and improve the efficiency of blowing, since lance position and oxygen flow are usually used as manipulated variables. The important parameters, determining heat and mass transport at the interface and in the liquid, are the interface shape, the width and depth of the cavity and the height of the peripheral lip, (Eletribi *et al.*, 1997), see Figure 1.

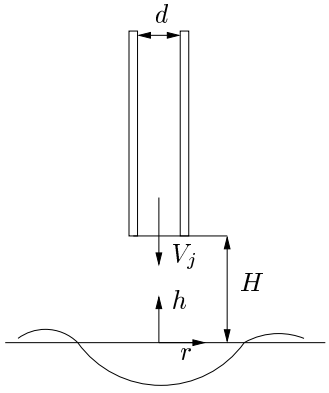

Fig. 1. Gas jet impinging on a liquid surface. The diameter of the lance is denoted by d, the maximum velocity of the gas V_j and H is the lance height above the liquid surface. h and r define the axes in the coordinate system.

Three different modes of the surface deformation have been identified in the process: dimpling, splashing and penetrating, (Molloy, 1970), depending on the properties of the gas jet and the liquid. The modes are illustrated in figure (2). Here the first two modes are considered.

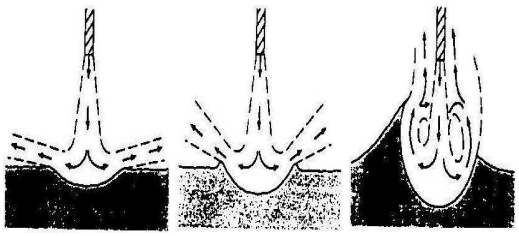

(a) (b) (c)

Fig. 2. Modes of surface deformation by the impinging gas jet. (a) Dimpling, (b) Splashing, (c) Penetrating.

Since the steel bath is a hostile environment for performing experiments, a water model is usually used to study the liquid cavity of the LD-converter. In the water model, the molten steel is simulated by water and compressed air is used instead of oxygen. The kinematic viscosity of water is similar to that of liquid steel, which means that the results from one can be transferred to the other. A significant advantage of the water model when it comes to shape estimation is that it is easy to collect visual information.

The first studies of the problem are reported in (Banks and Chandrasekhara, 1963), where experiments were performed, using a liquid-gas system consisting of water and air. Two approaches for analysing the phenomenon were explored, based on the assumption that the cavity is *stationary*. The first one related the depth of the surface depression or cavity to the stagnation pressure based on the centre line velocity of the jet in the neighborhood of the surface. The second one related the weight of the liquid displaced from the cavity to the momentum of the jet. It was found that the experimental data, obtained from photographs, were quite consistent with the theoretical results.

Later, experiments were performed using an air jet impinging on wet fast setting cement, (Cheslak *et al.*, 1969). In this way the width and height of the cavity could be easily measured. The conclusions made were: (i) the change in the vertical momentum of a jet impinging on a liquid surface is equal to the weight of displaced fluid; (ii) the depth and diameter of the cavity can be predicted; (iii) the cavity can be approximated by a paraboloid; (iv) there is a jet velocity over which splashing will occur and below which a smooth cavity exists; (v) liquid and gas viscosity and liquid surface tension do not affect the results. Cavity oscillations, both vertically and horizontally, were also observed in the water tank.

Analytical expressions were derived in (Turkdogan, 1966) for the depth and diameter of the cavity by considering the force on a unit area of the liquid surface, by using Newton's second law of motion. The pressure from the surface that counteracts this force is given by the maximum depression of the liquid. The predictions were validated on a system with different liquids and argon or nitrogen jet streams.

In an attempt to predict the whole cavity profile, a nonlinear singular integral equation was formulated in (Olmstead and Raynor, 1964), using conformal mapping methods and finite Hilbert transforms. The results were, however, limited to small angle depressions in the liquid surface. Later, new numerical procedures were developed, that allowed the depressions to be slightly deeper, (Vanden-Broeck, 1981) .

Energy and force balances were analysed in (Rosler and Stewart, 1968), to describe the indentation profile. These results were later used in (Berghmans, 1972), for a study of the stability of interfaces between fluids in motion, special attention being given to the role of surface tension. It was found that increasing surface tension has a stabilizing effect, while increasing the gas density or jet velocity is destabilizing.

More recently, experiments were carried out using a water-air system, (Eletribi *et al.*, 1997). Sophisticated image processing was used to measure the important parameters describing the cavity. The shape of the cavity was found to be either parabolic or Gaussian depending on the conditions of the jet flow and the liquid bath. The results were also compared to those found in (Banks and Chandrasekhara, 1963) and (Cheslak *et al.*, 1969). The comparison shows that they overestimated the cavity width and height because the theory did not properly account for the effects of the liquid viscosity and surface tension.

In this paper, the idea of combining image processing with a mathematical model of the cavity is taken further. Three following insights motivate the approach taken to obtain a description of the whole cavity, not only the depth and diameter.

- Mathematical models based on approximation techniques lack connection to the physics of the process and often lead to inconclusive results.
- A mathematical model of the liquid-gas jet system has to be rich enough in order to explain the cavity profiles observed in the water model.
- Dynamics of the temporal variations in the cavity depth and diameter have to be taken into account.

2. MATHEMATICAL MODELS

Mathematical modelling of the cavity is important to extract valuable information from the image in the face of disturbance. Due to the difficulties of estimating the form of the cavity, the researchers have concentrated on a few key parameters such as depth and diameter of the depression. Many suggestions on the cavity profile, such as paraboloid, ellipsoid or Gaussian form, have been made in the past, (Cheslak *et al.*, 1969), (Eletribi *et al.*, 1997). The results of approximation of an experimentally obtained cavity

profile by some of those functions are shown in Figure 3. As can be seen, the indentation is described equally well in the cavity itself, but the accuracy of the models differ when larger radial distances from the centre are considered. This means that the accuracy of approximation is mainly defined by the spatial interval at which the approximation is considered. Another problem with these models is that they lack physical insight into the process itself. Thus it is difficult to use them for any other purpose than image smoothing. For parameter, state estimation and control ends, more complex physically motivated models have to be considered. Hence, this paper focuses on a mathematical model stemmed from fluid dynamics, that, combined with image processing techniques, is used to estimate the whole cavity profile.

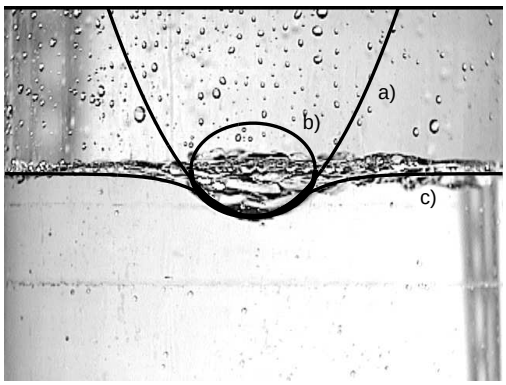

Fig. 3. Cavity approximations, (a) a paraboloid, (b) an ellipsoid and (c) an inverted hyperbolic cosine function.

2.1 Force balance

This subsection is based on the theoretical results obtained in (Rosler and Stewart, 1968). Since the width of the water tank is about 200 times the jet radius, the calculations presented here are for an axisymmetric jet impinging on a liquid in a container whose walls are at an infinite distance from the axis of symmetry. Using the coordinate system from Figure 1, an ordinary differential equation, describing the shape of the indentation can be written as follows:

$$\frac{d^2h}{dr^2} + \frac{\delta}{r}\frac{dh}{dr}\left[1 + \left(\frac{dh}{dr}\right)^2\right] = \frac{1}{\sigma}(p_1 - p_2)\left[1 + \left(\frac{dh}{dr}\right)^2\right]^{\frac{3}{2}} \tag{1}$$

with

$$p_1 - p_2 = \Delta p + (\rho_1 - \rho_2)gh \tag{2}$$

where g is the gravitational constant, Δp is the overpressure due to the impinging jet, δ =1, ρ_1 and ρ_2 are the densities of the liquid and the gas, respectively and σ is the surface tension of the specific liquid-gas combination.

To determine Δp, Rosler and Stewart used the experimental data of Gibson, for laminar jets impinging on a flat plate, (Gibson, 1934). The pressure distribution is approximated by:

$$\Delta p = \begin{cases} p_{max}\cos(0.826\frac{r}{r_j}) \text{ for } r \leq 1.2r_j \\ 4.53p_{max}\exp(-1.76\frac{r}{r_j}) \text{ for } r > 1.2r_j \end{cases} \tag{3}$$

where r_j is the jet radius, $p_{max} = \frac{1}{2}\rho_1 V_j^2$ is the jet strength and V_j is the maximum jet velocity.

In these experiments, (1) is used to approximate the measured cavity profile. The parameters defining the depth of the cavity, the surface tension σ and the parameter δ, are used as tuning parameters in the fitting of the model to the image frames. A loss function of the form

$$V(h(r), \hat{h}(r)) = \sum_{r=1}^{N}(h(r) - \hat{h}(r))^2 \tag{4}$$

where N is the number of edge pixels, h and $\hat{h}$ are the measured and calculated profile, respectively, is used as an optimization criterion for the estimation. By changing the parameter settings, the goal is to minimize the criterion and thus obtain a good description of the measured edge. Numerical studies of the loss function have been performed to evaluate the probability of converging to a local minimum. The probability was found to be small.

2.2 Stability analysis

The system described in (1) can be formulated in state-space form as

$$\frac{dx}{dr} = \begin{cases} x_2 \\ \frac{1}{\sigma}(\Delta p + (\rho_1 - \rho_2)gx_1)\left[1 + (x_2)^2\right]^{\frac{3}{2}} \\ \qquad -\frac{\delta}{r}x_2\left[1 + (x_2)^2\right] \end{cases} \tag{5}$$

where $x_1 = h$ and $x_2 = \frac{dh}{dr}$.

Since r is an integration variable in the state-space formulation and appears explicitly in the right-hand side of the equation, using a phase portrait is not feasible. A three dimensional plot of the evolution of (5) with increasing r, for different initial points, is shown in figure (4).

Taking into account that $\lim_{r\to\infty}\Delta p = \lim_{r\to\infty}\frac{\delta}{r} = 0$ the steady-state system is

$$\frac{dx}{dr} = \begin{cases} x_2 \\ \frac{1}{\sigma}((\rho_1 - \rho_2)gx_1)\left[1 + (x_2)^2\right]^{\frac{3}{2}} \end{cases} \tag{6}$$

The dynamics of (6) give rise to sustained periodic solutions.

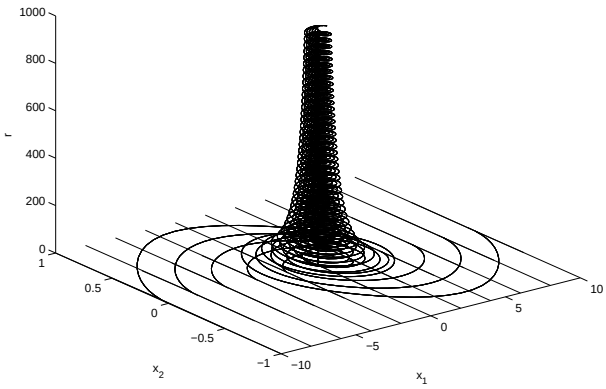

Fig. 4. Trajectories of the system with different initial values.

Proposition 1. Consider the function

$$V(x) = \frac{1}{(1+x_2^2)^{1/2}} - \frac{c}{2}x_1^2 \qquad (7)$$

where $c = \frac{1}{\sigma}(\rho_2 - \rho_1)g$, $c > 0$. Define a set M as the region $M = \{x \in \mathbb{R}^2 | c_1 \leq V(x) \leq c_2\}$, where $0 < c_1 < c_2 < 1$. Then there is a periodic solution of (6) in M.

Proof: Consider the system given by (6) and the function (7). The derivative of $V(x)$ along the trajectories of the system is given by

$$\dot{V}(x) = -cx_1\dot{x}_1 - x_2(1+x_2^2)^{-3/2}\dot{x}_2 = 0 \qquad (8)$$

Define a set M as the region

$$M = \{x \in \mathbb{R}^2 | c_1 \leq V(x) \leq c_2\} \qquad (9)$$

where $0 < c_1 < c_2 < 1$. Clearly M is bounded and positively invariant. It is also free of equilibrium points, since the only equilibrium point of the system is at the origin. Thus it follows from the Poincaré-Bendixson theorem, (Khalil, 1996), that there is a periodic solution of (6) in M. □

3. EXPERIMENTS

The experiments were conducted on a water model of the LD converter, previously used to study and control foaming, (Birk *et al.*, 2003). A single hole cylindrical nozzle with diameter 1.5 mm is used. The indentation profile arising when air is jetted onto the liquid surface is recorded in time using a CCD camera.

3.1 Video measurement

A digital video camera captures the cavity during the blow. The shoot angle of the camera can be easily changed. In these experiments the tank is filmed directly from the side of the water tank. In this manner a two-dimensional image is obtained. Since the jet-forming nozzle on the lance providing the gas is symmetric, the depression should be rotation symmetric. To extrapolate into three dimensions, the two dimensional image is rotated. The video camera produces a sequence of image frames that is the information source in the estimation of the cavity shape and can as well be used to obtain a temporal profile.

3.1.1. Camera calibration The frames collected from the video camera are represented by pixel values. It is desirable to express the axis of the images in length units and thus a conversion between the two is performed. Special care is also taken to compensate for a tilted image, due to the camera setting.

3.1.2. Light settings In photography, the lighting has to be designed beforehand to obtain the best imaging results. This is especially important for image processing purposes. The lighting has to suit the camera and the purpose of filming or else the image can be useless. Faulty light settings result in shadows, glares and unwanted reflections in the water surface. In these experiments the water tank was lit from the side with a reflector behind, which is proven to provide the best lighting conditions.

3.2 Image processing

To extract the edges from the image an in-house software is used. The frames of the video sequence are filtered to reduce the noise in the image. Then edge detection is applied using a thresholding method, together with some basic image processing tools such as opening, closing and flood-fill, (Sonka *et al.*, 1999).

4. RESULTS

In this section the results for the indentation profile are presented. First the results of edge detection in the video frames are presented. Then the data obtained is used to draw conclusions about the temporal behavior of the cavity.

4.1 Image processing results

The measurements are given in the form of images obtained by a video camera. To be able to compare the image with a mathematical function, the edge of the cavity is extracted from the measurement. The result of such a procedure is shown in Figure 5.

The lower edge is used as a description of the cavity in the image. Optimizing the parameters in the mathematical model leads to the model fit shown in Figure 6. As can be seen, the model is flexible enough to explain the profile well. In Figure 7 the calculated profiles

have been superimposed on the image from the video camera.

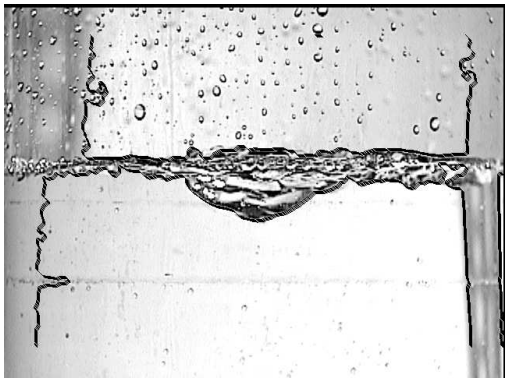

Fig. 5. Detected edges in the image.

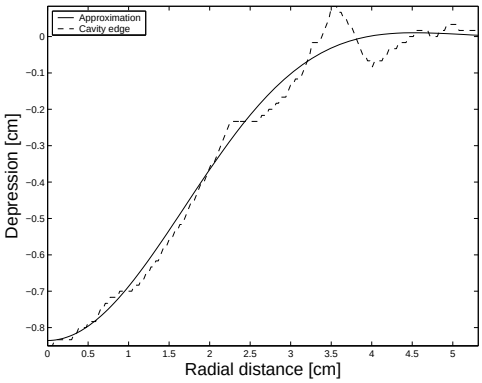

Fig. 6. Approximation of the cavity profile using (a) a mathematical model based on force balance. The approximated cavity is shown together with the measured edge.

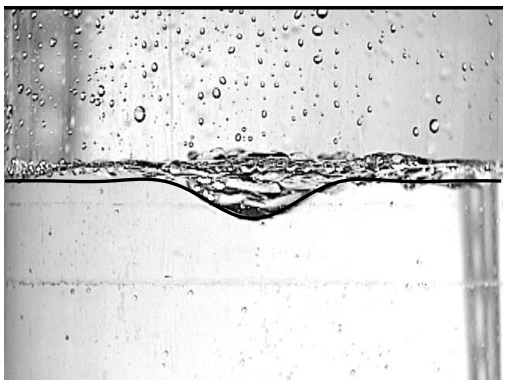

Fig. 7. Approximation of the cavity profile for (a) a mathematical model based on force balance. The approximated cavity is superimposed on an image frame.

4.2 Depth estimation

The centerline depth of the cavity was estimated for a sequence of 900 frames. The mean depth and the standard deviation are shown in Figures 8 and 9 for different lance heights and gas flow rates.

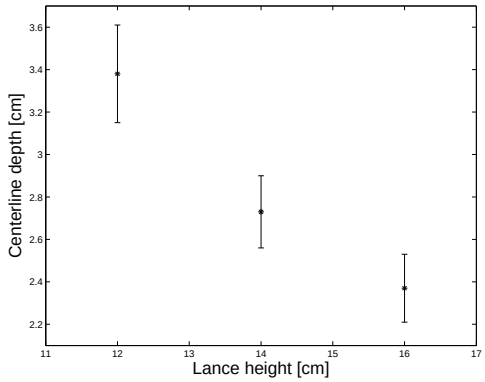

Fig. 8. Mean depth and standard deviation for different lance heights and constant gas flow rate, 21 l/min.

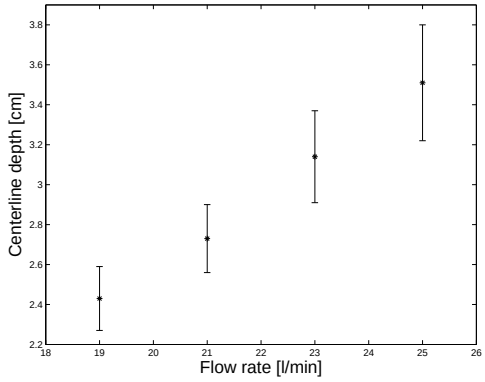

Fig. 9. Mean depth and standard deviation for different gas flow rates and constant lance height, 14 cm.

As can be seen in Figure 8, for a constant gas flow rate the depth of the cavity decreases with increasing lance height until no cavity forms on the water surface. The uncertainty of the estimate decreases with increasing lance height. For a constant lance height, Figure 9, the depth of the cavity increses with increasing gas flow rate. Also the uncertainty of the estimate increases due to the increasing disturbance (bubbles, splashing) in the images.

4.3 Cavity oscillations

The estimate of the cavity depth is obtained from the mathematical models, in each frame. Since the force balance model does not account for the cavity oscillation, the assumption that the process is stationary leads to large variance of the estimates.

The frequency content of the oscillations is studied using the Fast Fourier Transform (FFT). In Figure 10 the FFT of two different lance heights, with the same gas flow rate is shown. The oscillative behavior of the cavity for the same lance height, but with two different gas flow rates, is characterized in Figure 11 by means of the FFT.

As can be seen in Figures 10 and 11, the frequency of the cavity oscillations seem to be located over a band of frequencies from $3.5 - 6$ Hz and depending

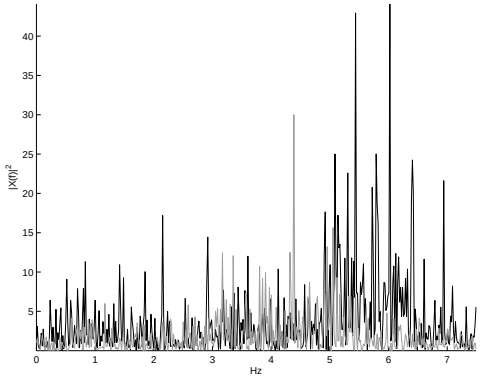

Fig. 10. FFT of depth estimates with lance height 12 cm (black) and 16 cm (light gray) with gas flow rate 21 l/min.

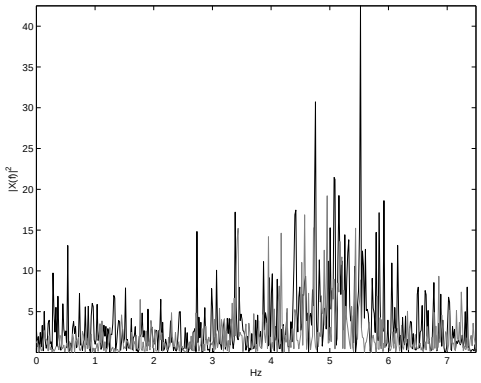

Fig. 11. FFT of depth estimates with gas flow rate 23 l/min (black) and 19 l/min (light gray) with lance height 14 cm.

on the gas flow rate and the lance height, the spectrum is shifted slightly towards higher or lower frequencies. The cavity depth is a periodic signal over time, of a complex waveform and not easy to model.

5. CONCLUSIONS

An experimental and theoretical study of blowing in an LD-converter water model has been carried out. A video camera is used to measure the indentation profile of the cavity, during the blow. Image processing tools together with a mathematical model are used to estimate the cavity profile. More sophisticated and physically motivated models explain better the observed cavity form.

The uncertainty of the cavity depth estimates was quantified and the oscillative behavior of the depression was studied using the Fast Fourier Transform.

The results of this research will hopefully provide a tool for the metallurgists to obtain deeper insight in the physics of top blowing.

6. ACKNOWLEDGEMENTS

This work has been in part supported by The Swedish Steel Producers' Association and by the EC 6th Framework programme as a Specific Targeted Research or Innovation Project (Contract number NMP2-CT-2003-505467). The authors also wish to thank the Department of Process Metallurgy of the Royal Institute of Technology, Stockholm, for allowing the authors to use their experimental facilities, Jimmy Tila for help with experiments and software, and Professor Vladimir Pavlenko of Uppsala University for sharing his vast knowledge of wave theory.

REFERENCES

Banks, R.B. and D.V. Chandrasekhara (1963). Experimental investigation of the penetration of a high-velocity gas jet through a liquid surface. *Journal of Fluid Mechanics* **15**(103), 13–34.

Berghmans, J. (1972). Theoretical investigation of the interfacial stability of inviscid fluids in motion, considering surface tension. *Journal of Fluid Mechanics* **54**, 129–141.

Birk, W., I. Arvanitidis, P. Jonsson and A. Medvedev (2003). Foam level control in a water model of the LD converter process. *Control Engineering Practice* **11**, 49–56.

Cheslak, F.R., J.A. Nicholls and M. Sichel (1969). Cavities formed on liquid surfaces by impinging gaseous jets. *Journal of Fluid Mechanics* **36**, 55–64.

Eletribi, S., D.K. Mukherjee and V. Prasad (1997). Experiments on liquid surface deformation upon impingement by a gas jet. In: *Proceedings of the ASME Fluids Engineering Division*. Vol. 244.

Gibson, A.H. (1934). *Hydraulics and Its Application*. London:Constable.

Khalil, H.K. (1996). *Nonlinear systems*. Prentice-Hall, Inc.

Molloy, N.A. (1970). Impinging jet flow in a two-phase system:the basic flow pattern. *Journal of the iron and steel institute* pp. 943–950.

Olmstead, W.E. and S. Raynor (1964). Depression of an infinite liquid surface by an incompressible gas jet. *Journal of Fluid Mechanics* **19**, 561–576.

Rosler, R.S. and G.H. Stewart (1968). Impingement of gas jets on liquid surfaces. *Journal of Fluid Mechanics* **31**, 163–174.

Sonka, M., V. Hlavac and R. Boyle (1999). *Image processing, analysis and machine vision*. PWS Publishing.

Turkdogan, E.T. (1966). Fluid dynamics of gas jets impinging on surface of liquids. *Chemical Engineering Science* **21**, 1133–1144.

Vanden-Broeck, J.M. (1981). Deformation of a liquid surface by an impinging gas jet. *SIAM Journal of Applied Mathematics* **41**(2), 306–309.